Coastal Engineering 168 (2021) 103949

Contents lists available at ScienceDirect

Coastal Engineering

journal homepage: www.elsevier.com/locate/coastaleng

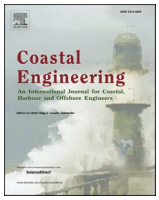

Standing longwave formations in reef-lagoon bathymetries

Vivek A. Bheeroo, Harry Yeh *

Oregon State University, School of Civil and Construction Engineering, USA

ARTICLE INFO

Keywords:
Reef
Lagoon
Long wave
Standing wave
Cnoidal wave
Runup

ABSTRACT

Standing longwave formations are investigated in the presence of a broad submerged sill off the vertical reflective wall: this configuration represents a model of reef-lagoon formations often present in coral-reef coasts. A series of laboratory and numerical experiments are performed for the waves of which wavelengths are comparable to the bathymetry length scale. The results reveal that the wave amplitude at the reflective boundary wall can surpass the case without the presence of the reef. Adverse wave conditions are also observed in the reef-lagoon span when the waves are longer than the reef breadth. Enhancement of the higher harmonics of the waves is seen inside the lagoon. The present experimental results highlight the potential that the presence of an offshore reef could worsen the wave climate in the nearshore region behind the reef for the case of standing longwave formations. The zone of influence of the reef is however localized to the lagoon and the reflective wall extent, while the offshore standing wave formation remains minimally influenced except for the phase shift in the standing-wave envelope.

1. Introduction

Coral reefs play a significant role in the protection of shorelines. Their buffering properties on energetic offshore waves are well recognized and reported in meta-analyses, such as (Ferrario et al., 2014). What we attempt to determine here is if such coral-reef protection is also effective for very long incident waves: e.g., swells and tsunamis. Among reefs, we specifically focus on the conditions of which the offshore reef is broad and detached from the shore by a deeper-depth lagoon with a comparable breadth. Such bathymetric configurations are found in some tropical oceanic islands. For example, Fig. 1a shows an example of such in Mauritius: both breadths of the reef and the lagoon are approximately 2 km. Similar reef-lagoon configurations can be found in Seychelles (Fig. 1b) and Fiji (Fig. 1c). In particular, we investigate the standing wave formations off the vertical reflective wall: this configuration represents a simplified model of coral-reef coasts with a steep-slope shoreline or the presence of man-made seawall. We consider the incident long waves with the length scale being comparable with or longer than the scale of the reef-lagoon system.

To explore the wave-response mechanisms, we use a simplified bathymetry as will be discussed in Sec. 3. Laboratory experiments are performed to explore the long-wave response, and the data are used to ensure the performance of the numerical model. Then, a series of numerical experiments are performed for the extended conditions that are not possible to be realized in the laboratory. The objective of this study is to understand the long-wave response in the broad reef-lagoon system in which the length scales of the incident wave (i.e., wavelength) and the bathymetry (i.e., distance between the offshore limit of the reef and the shoreline) are comparable. It is noted that the outcomes should be applicable to smaller scale situations, such as the cases of broad detached and submerged breakwaters.

2. Background

While there are many previous studies reported on wave response in coral reefs (Hardy and Young, 1996; Lee and Black, 1978; Longuet-Higgins and Stewart, 1960, 1964; Lowe et al., 2005; Nwogu and Demirbilek, 2010; Péquignet et al., 2009, 2011; Seelig, 1983; Young, 1989), the present type of reef-lagoon system with wide breadth has not been studied extensively in the past. On the other hand, there are many studies on the topic of wave transmission across and behind man-made submerged breakwaters (Adams and Sonu, 1987; d'Angremond et al., 1997; Goda et al., 1967; Johnson et al., 1951; Petti and Ruol, 1993; Seabrook and Hall, 1999; van der Meer et al., 2005). Of note, Dick and Brebner (1969) investigated the performance of submerged obstacles on dissipating energetic incident waves. The major attenuation observed was linked to turbulence and wave breaking phenomenon. They observed that an important portion of the transmitted energy across the

* Corresponding author. School of Civil & Construction Engineering, Oregon State University, Corvallis, OR, 97331, USA.
E-mail address: harry@oregonstate.edu (H. Yeh).

https://doi.org/10.1016/j.coastaleng.2021.103949
Received 2 September 2020; Received in revised form 29 May 2021; Accepted 20 June 2021
Available online 21 June 2021

obstacle was transferred to higher frequencies. This observation aligned with the findings of Goda et al. (1967), who reported higher harmonic generation in the transmitted waves. This transfer of energy from the fundamental frequency to the higher harmonics was also noted by Dattatri et al. (1979), while investigating waves across breakwaters of diverse cross-sectional geometries. The generation of higher harmonics by submerged structures is one of the two major phenomena that arise in nature, with the other being the production of vortices, owing to the flow separation. Massel (1983) and Rey et al. (1992) confirmed the generation of higher harmonics for the cases of nonlinear waves traversing a submerged obstacle. In similar studies, Eldeberky and Battjes (1995) noted that on the seaward side of the obstacle, there is an amplification of the harmonics that are bound to the fundamental harmonic. On the shoreside, as the waves penetrate the deepening region, the decreasing nonlinearity releases the harmonics as free waves. To complement these findings, Huang and Dong (1999) showed that, while the waves pass above the structure, the order of magnitude of the amplitude of the bound and free modes are similar.

Most of the numerical exercises carried out for waves propagating across submerged structures have used the Boussinesq type equations (Losada et al., 1996). Beji and Battjes (1994) used a Boussinesq model to validate their early laboratory findings (Beji and Battjes, 1993) for wave transformation across a submerged trapezoidal-shaped structure. Their results are consistent with Eldeberky and Battjes (1995), who employed the Boussinesq equations for their numerical tank. The evolution of the higher harmonics on a spatial scale is seen to amplify progressively and become more apparent on the lee side of the structure.

The Boundary Element Method (BEM) based on the Euler formulation was applied to the problem for waves over submerged obstacles. Of note, Kittitanasuan et al. (1993) were amongst the first to utilize this method to solve the wave field for incident waves across a submerged step. They noted the enhancement of 2^{nd} and 3^{rd} harmonics, which they identified as the main mechanism behind the strong nonlinearity, as noted in (Beji and Battjes, 1994). Ohyama and Nadaoka (1994) employed the BEM method to solve for the nonlinear waves across a rectangular step. They noted that, for the case where the width of the step is half of the wavelength over the step, increase in the higher harmonics is observed to reach maximal magnitudes.

Li and Ting (2012) captured the wave field in the presence of a submerged rectangular step in the laboratory. In the case of monochromatic waves, they found that the wavelengths of the generated harmonics vary in space due to nonlinear wave-wave interaction in space. Li and Ting (2012) also reported a shift in phase of successive crests within the wave propagation. They speculated that the observed phase shift was attributed to the fact that the fundamental harmonic catches up with the 2^{nd} free harmonic owing to discrepancies in phase speeds within the wave train propagation. The role of surf zone width on the ensuing resonance response at the shoreface has also been investigated. Baldock et al. (2004) varied the surf zone width by varying the wave height and water level over a bar crest. They found that the presence of the bar induces a frequency downshift in the spectral peak of radiated long waves. They attributed this observation to the increased surf zone width.

The bulk of the previous studies on the topic of wave transformation across a submerged obstacle have explored the attenuating effects on relevant parameters, such as maximum water surface elevation, wave heights, and in a few cases, kinematics and wave forces. These studies also examined the role of higher harmonic generation in promoting nonlinearity in the water profile. The complex problems within the examined literature were simplified by implementing an absorbing slope at the downstream end of the obstacle. The increased complexity of the system is noted in the case of a vertical reflective boundary at the downstream end from preliminary studies on the topic (Monsalve et al., 2015; Zheng et al., 2007). The vertical boundary on the lee of the structure is suggested to result in different solutions to the classic problem of wave propagation across a submerged structure bounded by an absorbing boundary. Zheng et al. (2007) stated that this is due to the influence of the reflective boundary on the structure. Monsalve et al. (2015) identified the generation of complex behavior from spectral analysis of the captured surface data. They observed resonance for fixed frequencies, while stating that the presence of nonlinearities and harmonics generation propose pertinent questions that should be treated in future works.

The goal of this study is to extend the analysis of waves traversing a submerged structure by imposing a vertical reflective wall immediately downstream of the lee of the structure. The present study fills gaps in the literature for the cases where long waves traverse a fully submerged, broad-crested reef, and penetrate into a lagoon. The generated standing-wave envelope, owing to the reflections from the end-wall, is analyzed, and the effect of lagoon breadth on possible resonance response is also examined. We consider our study to be of an exploratory nature, as distributions of wave phases and amplitudes in the real lagoon-reef systems are unpredictable.

3. Methods

The present investigation is conducted in two parts. Firstly, a series of laboratory experiments are undertaken, which are then used for the validation of a numerical code. Secondly, the numerical code is used to conduct additional experiments.

3.1. Laboratory experiment

Laboratory experiments are performed in a wave tank, which is 7.3

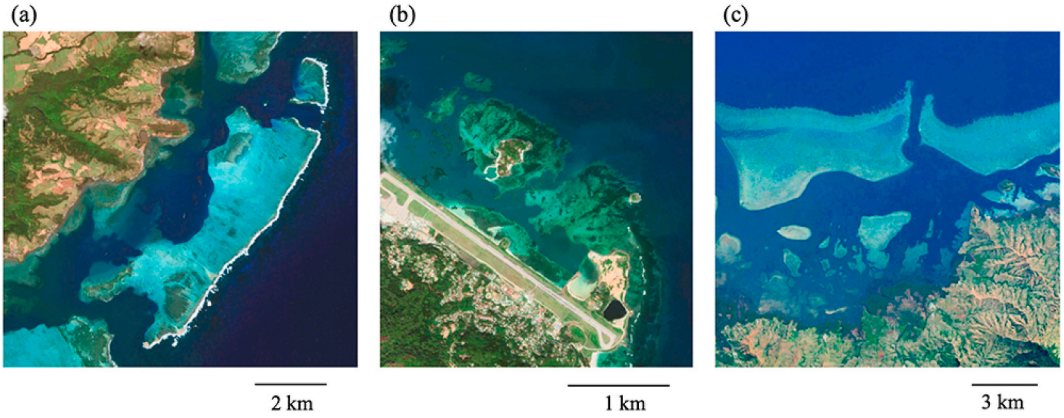

Fig. 1. Typical formation of broad-crested reef and lagoon: (a) Mauritius (20°22′S, 57°45′E); (b) Seychelles (4°40′S, 55°31′E); (c) Fiji (17°20′S, 177°59′E). The images are taken from Google Earth.

m long, 2.5 m wide, and 0.30 m deep. The schematic drawings are shown in Fig. 2. A wave-maker system is equipped at one end of the tank, and the wave paddle is pushed horizontally in piston-like motion by the linear motion device. The precision setting and the performance of the wavemaker system can be found in (Ko and Yeh, 2018).

The submerged broad sill that is a model of the reef, is $D = 0.0254$ m high and $L_R = 0.3175$ m wide, spanning 2.5 m between the side walls. The sill is placed $L_L = 0.43$ m from the end-wall (see Fig. 2b). The experiments are performed with the still water depth $h_0 = 0.05$ m. From hereinafter, for convenience, we call the submerged broad sill "the reef" and the space between the sill and the end-wall "the lagoon". The end-wall marks the start of the cross-shore, normalized reference system x/L_R, with x being the distance from the end-wall, pointing to the offshore direction.

Three acoustic wave gages (General Acoustics, Model HF54 Controller and USS 02-HF Sensors) are used to measure the temporal variations of water-surface elevations at the locations shown in Fig. 2. The sampling rate is set at 50 Hz and the gage resolution is 0.18 mm. Taking advantage of the precisely repeatable laboratory system (Ko and Yeh, 2018), the wave data are obtained by traversing two of the gages equipped on the carriage. The third gage is kept fixed at the offshore location (Sta. 1) to monitor the repeatability of the experiments. In addition, a high-resolution video camera (AOS, Model Q-PRI, 1696 × 1710 pixels resolution) is used behind the end-wall to capture the wave run-up at the sampling rate of 63 Hz through the transparent glass-plate wall.

Since our focus is on the response of long waves to the reef-lagoon system, we impose cnoidal waves as the incident waves. Cnoidal waves are an exact periodic solution to the Korteweg-de Vries (KdV) equation that models weakly nonlinear weakly dispersive waves. In terms of the departure of the water-surface from the quiescent state η, the cnoidal waves can be expressed as

$$\eta = -\eta_2 + (\eta_1 + \eta_2)cn^2\left\{\left[\frac{3(\eta_1+\eta_3)}{4h_o^3}\right]^{\frac{1}{2}}(x - Vt)\middle| m\right\}, \tag{1}$$

in which

$$m = \frac{\eta_1 + \eta_2}{\eta_1 + \eta_3}, \tag{2}$$

$$\lambda = \left[\frac{16h_o^3}{3(\eta_1+\eta_3)}\right]^{\frac{1}{2}} K(m), \tag{3}$$

$$\eta_3 = \eta_1\left\{\frac{E(m)}{K(m) - E(m)}\right\}, \tag{4}$$

$$V = \sqrt{gh_0}\left[1 + \frac{1}{2}\left(\frac{\eta_1 - \eta_2 - \eta_3}{h_o}\right)\right], \tag{5}$$

where x is the propagation coordinate, t is time, g is the gravity, h_0 is the initial water depth, η_1 is the crest amplitude, η_2 is the trough amplitude, $H = \eta_1 + \eta_2$ is the wave height (vertical difference between crest and trough), V is the wave celerity, $K(m)$ and $E(m)$ are the complete elliptical integrals of the first and second kind with the elliptic parameter m, respectively, and λ is the wavelength. Note that η_3 is one of the roots of the cubic polynomial associated with the elliptic function solutions for cnoidal waves (Mei, 1983). The waveform is specified once a crest amplitude η_1 and a wavelength λ are chosen. Note that the cnoidal wave approaches to that of linear monochromatic wave as $m \to 0$, and that of a solitary wave as $m \to 1$. For the laboratory experiments, three cnoidal waves are tested as listed in Table 1. For all three cases, the target incident wave height, H_i, is 1.0 cm in the still water depth $h_0 = 5.0$ cm. The motion of the wave paddle is set to match the depth-averaged wave velocity with the use of the algorithm in Goring and Raichlen (1980).

Table 1
Summary of target wave properties for the waves used in the laboratory experiments.

Case	Still water depth, h_o (cm)	Incident wave height, H_i (cm)	Wavelength, λ (m)	Period, T (s)	Elliptic parameter, m
A	**5**	**1**	**0.3175**	**0.538**	**0.457**
B	**5**	**1**	**0.6350**	**0.925**	**0.902**
C	**5**	**1**	**0.7938**	**1.130**	**0.968**

Note that the wavelength λ for Case A matches the reef breadth and is progressively increased for Cases B and C. It is reminded that our focus in this study is long waves: λ is comparable to the geometric horizontal scale. As λ increases for a given wave height, the nonlinearity effects become more prominent, as indicated by the values of elliptic parameter m.

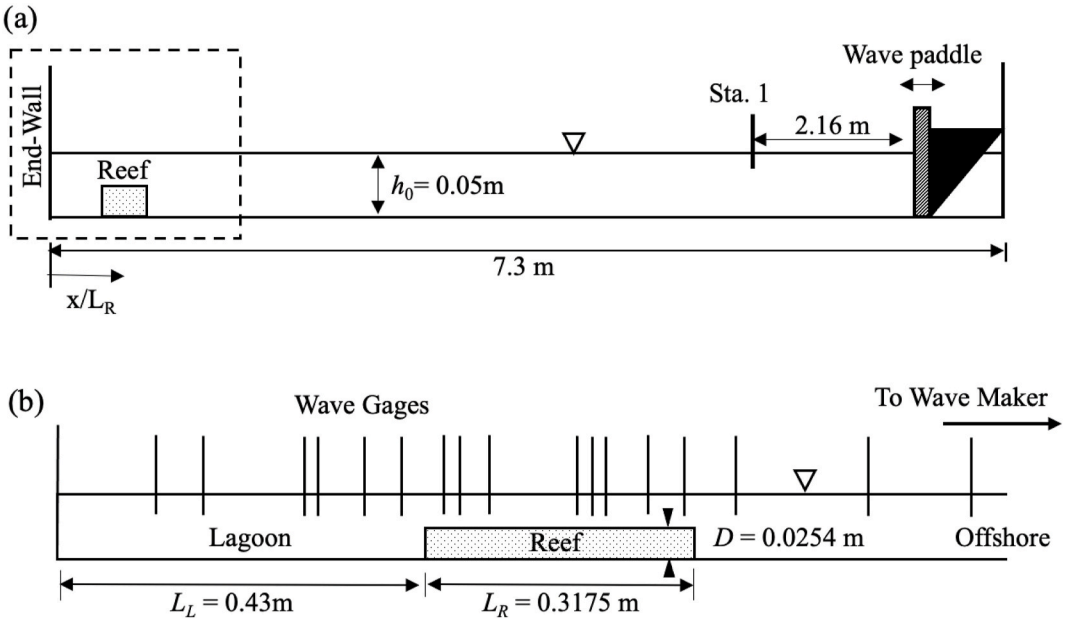

Fig. 2. Schematic drawings of the wave tank: (a) elevation view showing the position of offshore reference wave gage (Sta.1); (b) closeup view of the lagoon-reef system placed near the end of the tank (the vertical lines show the locations of the wave gages). Note that the basin width in the alongshore direction is 2.5 m.

The laboratory experiments are carried out for the duration of approximately 30*s*, then the wavemaker is stopped. This ensures that sufficient water-surface data can be acquired without contamination by re-reflection from the wave maker. For example, Fig. 3 shows the extraction of the steady wave-amplitude state of the time-series data, in order to obtain the standing wave envelope. The steady wave-amplitude data is then used to construct the maxima and minima of the wave envelope. This was accomplished by averaging the wave-crest peaks at a given cross-shore location to obtain the maximum. The same procedure is applied to obtain the envelope minima using the wave-troughs.

3.2. Numerical experiment

The data from the laboratory experiments are used to examine the performance of the numerical model. Here we utilize an open-source software, Celeris (Tavakkol and Lynett, 2017), which is a solver for the Boussinesq-type equations using the finite volume method. For the purpose of the present problem, we consider 1D wave propagation in the frictionless horizontal bed. The governing equations – conservations of mass and momentum – used in Celeris can be written, respectively, as:

$$\partial_t h + \partial_x(h\bar{u}) = 0, \tag{6}$$

$$\partial_t(h\bar{u}) + \partial_x(h\bar{u}^2) + gh\partial_x h = \frac{6}{15}h_o^2\partial_{xxt}(h\bar{u}) + \frac{1}{15}gh_o^3\partial_{xxx}\eta, \tag{7}$$

where $h = h_0 + \eta$ is the total water depth and $\bar{u}$ is the depth averaged horizontal velocity. The detailed description for the governing equations and the model validations are presented in Tavakkol and Lynett (2017).

The domain of the laboratory experiments (Fig. 2) is replicated on Celeris, discretized with 715 cells in the *x*-direction, such that each cell represents 1 cm in the physical tank, ranging from the wave paddles to the vertical end-wall (Fig. 2a). The end-wall is set to be completely reflective. Cnoidal waves are generated at the upstream boundary. Fig. 4 presents the performance of numerically generated cnoidal wave in Celeris. It is seen that the resulting wave profile is in excellent agreement with the theoretical profile (1): Root Mean Square Error (RMSE) in terms of the local wave height is about 1% of the still water depth.

The similar procedure is used to extract the standing-wave envelope for the numerical timeseries data. As shown in Fig. 5, the numerically simulated results are in good agreement with those obtained in the laboratory (RMSE of $H/h_0 = 0.0268$, 0.0263 and 0.0280 for Cases A, B and C, respectively). The performance of Celeris provided us with confidence to pursue the numerical experiments for expanded cases beyond the laboratory conditions.

Table 2 shows the cases of the numerical experiments: note that R1LA, R1LC, and R1LE correspond to A, B, and C, respectively (see Table 1), of the laboratory experiments. The numerical experiments include the setup without a reef. Such cases are used for the comparison with the corresponding cases influenced by the presence of the reef. Taking advantage of the numerical experiments, we simulate the waves in a longer tank, 25 m long: recall that our laboratory tank is 7.3 m long. The domain is discretized with 2 500 cells in the *x*-direction, such that each cell along the cross-shore direction represents 1 cm in the tank: the identical resolution was used for the simulations of the laboratory cases as discussed earlier. The longer propagation span allows us to obtain the data for a longer duration, approximately 80 s, without contamination from the re-reflected waves from the offshore boundary. The reef and lagoon dimensions are kept unchanged from those shown in Fig. 2. The target incident wave height, $H_i/h_0 = 0.2$, is also kept the same as that of the laboratory experiments. No friction effect is included in the model.

4. Results and discussion

4.1. Wave envelopes

As explained in Sec. 3, the standing wave envelope is constructed from the steady wave-amplitude state portion of the data. First, we present the results for Cases R1LA, R1LC and R1LF (see Table 2), and compare the wave envelopes with the ones formed in the absence of the reef (Cases LA, LC and LF, respectively). It is reiterated that the presented results are for nonbreaking wave conditions. The wave harmonic analysis is performed: the stationary time-series data are decomposed to the wave amplitudes corresponding to the 1st (fundamental), 2nd and 3rd harmonic components with the use of the built-in MATLAB Fast Fourier Transform (FFT) routine. Note that the amplitudes for the 4th harmonic and higher are insignificant and hence not included. The harmonic analysis for the cases without a reef display uniformity, demonstrating that the wave conditions reached steady state: see Figs. 6b, 7b and 8b.

Cases LA and R1LA are presented in Fig. 6: recall that those are generated by the incident cnoidal waves with the elliptic parameter $m = 0.457$ and the wavelength of the incident waves matches the breadth of the reef ($\lambda = L_R$). In the wave envelope plot in Fig. 6a, substantial amplitude attenuation is seen inside the lagoon region in comparison to the ones in Case LA. The reef is effective in blunting the incident wave energy, leading to a reduced wave runup and rundown at the end-wall: reduction of H at the end-wall is approximately 34%. The envelope

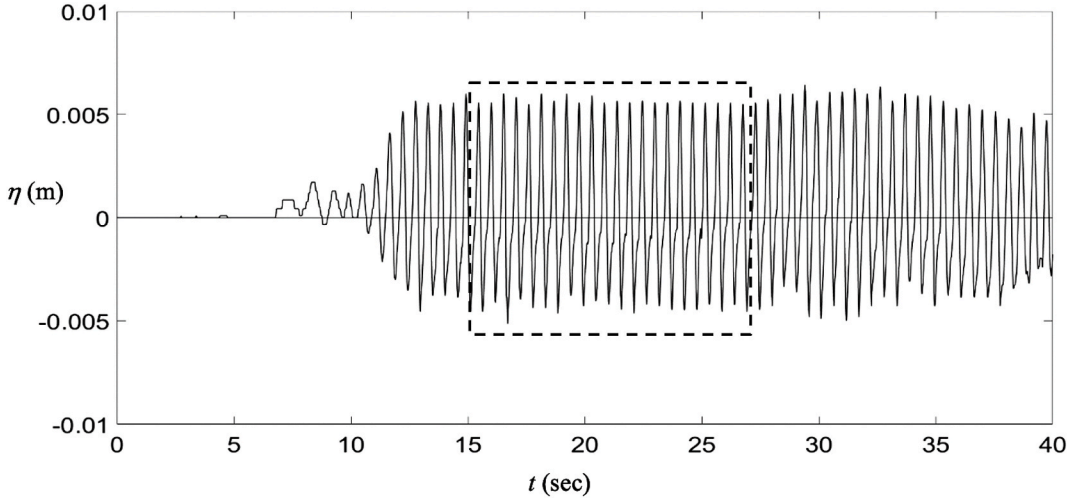

Fig. 3. Wave gage data taken in the lagoon. Only the wave response at the steady wave-amplitude state is used for the analysis, excluding the initial longwave noise and the developing stage, as well as the contamination caused by the re-reflected waves from the wavemaker. The analysis is made with the data in the time interval indicated in the dashed inset.

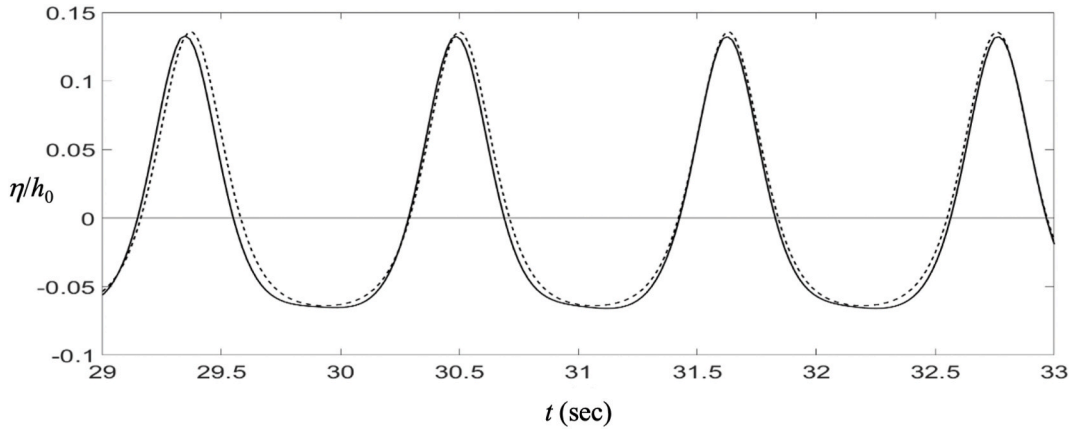

Fig. 4. Comparison of incident wave profiles from numerical experiments, solid line, with theoretical cnoidal wave profiles from (1), dashed line.

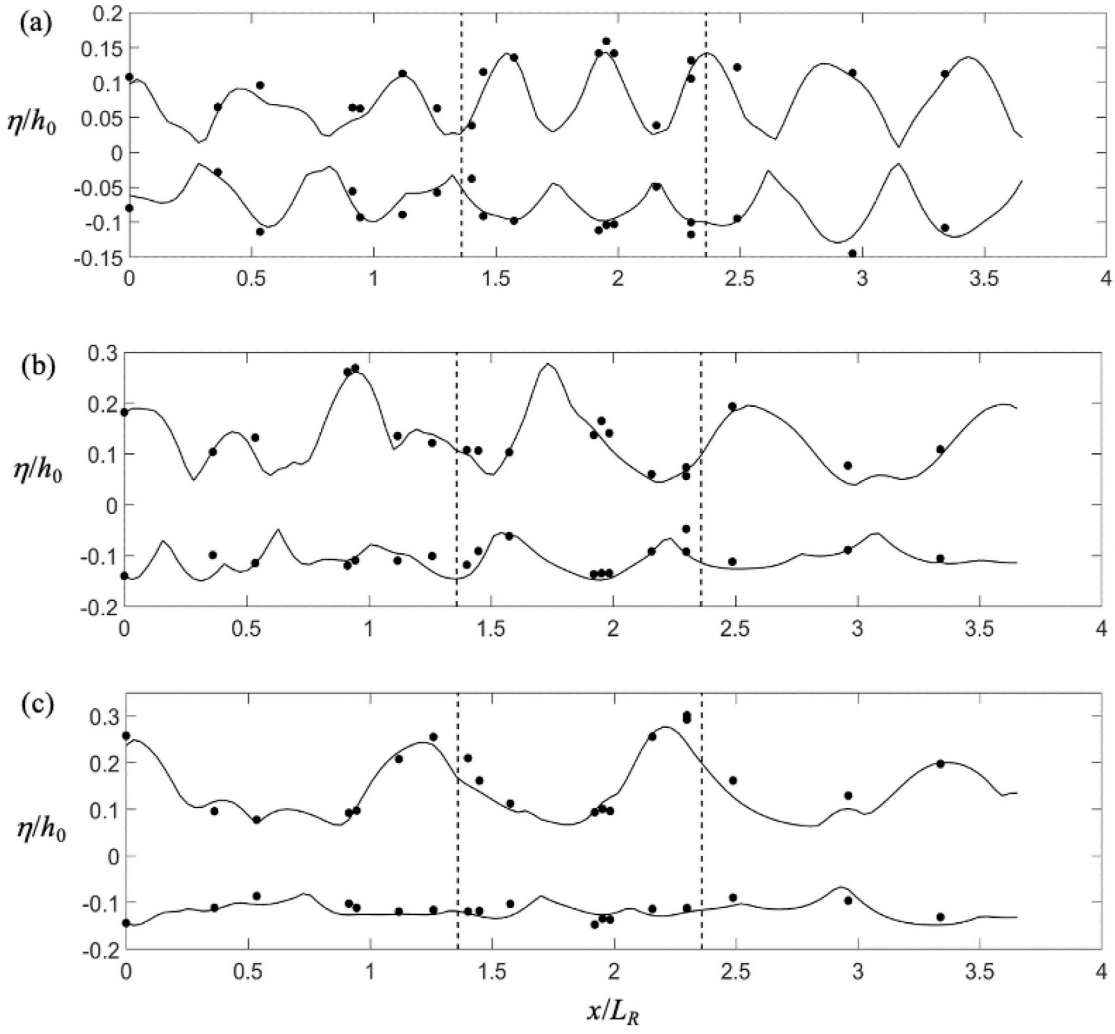

Fig. 5. Wave envelopes of standing waves in the lagoon-reef system for the wave conditions listed in Table 1: a) Case A (b) Case B, and (c) Case C. Solid lines, numerical results; dots, laboratory data; RMSE of $H/h_0 = 0.0268$, 0.0263 and 0.0280 for Cases A, B and C, respectively. The location of the reef L_R is marked by the vertical dotted lines.

peaks along the reef are of a similar magnitude to the ones in Case LA, while the troughs, on the other hand, are reduced by 23% approximately. It appears that, though the maximum water-surface elevations remain unchanged, the asymmetry of the envelope increases on the reef due to the reduction of water depth, transforming into features of more peaked crests and flattened troughs. A node is observed at the inshore edge of the reef, with the offshore edge displaying an anti-node formation. This contrasts with the node formations at both edges of the reef for Case LA, representing the incident cnoidal wavelength that is the same as the reef breadth. The shallower water depth over the reef affects the

Table 2
Extended matrix and naming convention for numerical experiments.

	Wavelength, λ (m)					
Reef height, D	L_R , $m = 0.457$	$1.5L_R$, $m = 0.742$	$2.0L_R$, $m = 0.902$	$2.25L_R$, $m = 0.943$	$2.5L_R$, $m = 0.968$	$3.0L_R$, $m = 0.990$
No Reef	**LA**	**LB**	**LC**	**LD**	**LE**	**LF**
$0.508h_o$	**R1LA**	**R1LB**	**R1LC**	**R1LD**	**R1LE**	**R1LF**
$0.6h_o$	**R2LA**	**R2LB**	**R2LC**	**R2LD**	**R2LE**	**R2LF**
$0.7h_o$	**R3LA**	**R3LB**	**R3LC**	**R3LD**	**R3LE**	**R3LF**

wavelength, consequently, causing the phase shift in the offshore wave envelope of Case R1LA. The envelope shape is seen to regain uniformity in the offshore region, which closely matches the shape of Case LA, albeit with slightly smaller peaks and troughs (about 8% reduction for both the peaks and troughs). The uniform, repeated patterns in the wave envelope in the offshore region indicates that the reef influence is somewhat limited to the vicinity of the reef location. The fairly symmetrical pattern about the still water level present in the uniform offshore envelope further attests to the smallness of the nonlinearity effect. The cnoidal waves display near-sinusoidal waveform, which is further supported by the value of parameter $m = 0.457$.

The harmonic analysis for LA and R1LA is presented in Fig. 6b and c, respectively. For the case without a reef, the fundamental harmonic dominates the higher harmonics consistently across the domain. This reflects the near-linear incident wave characteristics. The presence of a reef (Fig. 6c) causes a slight reduction in the offshore fundamental harmonic amplitudes from Case LA (Fig. 6b). The peaks are uniform in the offshore region, up until the reef, where a gradual attenuation is observed. This attenuation corresponds with an increase in the 2nd harmonic component along the reef. The resurgence in the 3rd harmonic amplitude is observed, albeit to a lesser extent. The fundamental harmonic amplitude is further reduced inside the lagoon region, while the 2nd harmonic amplitude remains relatively unchanged. The results indicate the energy transfer to the higher harmonics for the transmitted waves across the reef.

The envelopes for Cases LC and R1LC are shown in Fig. 7a: this is the case for the incident cnoidal wave with $m = 0.902$ and the wavelength is twice the reef breadth ($\lambda = 2\,L_R$). The wave activity inside the lagoon is

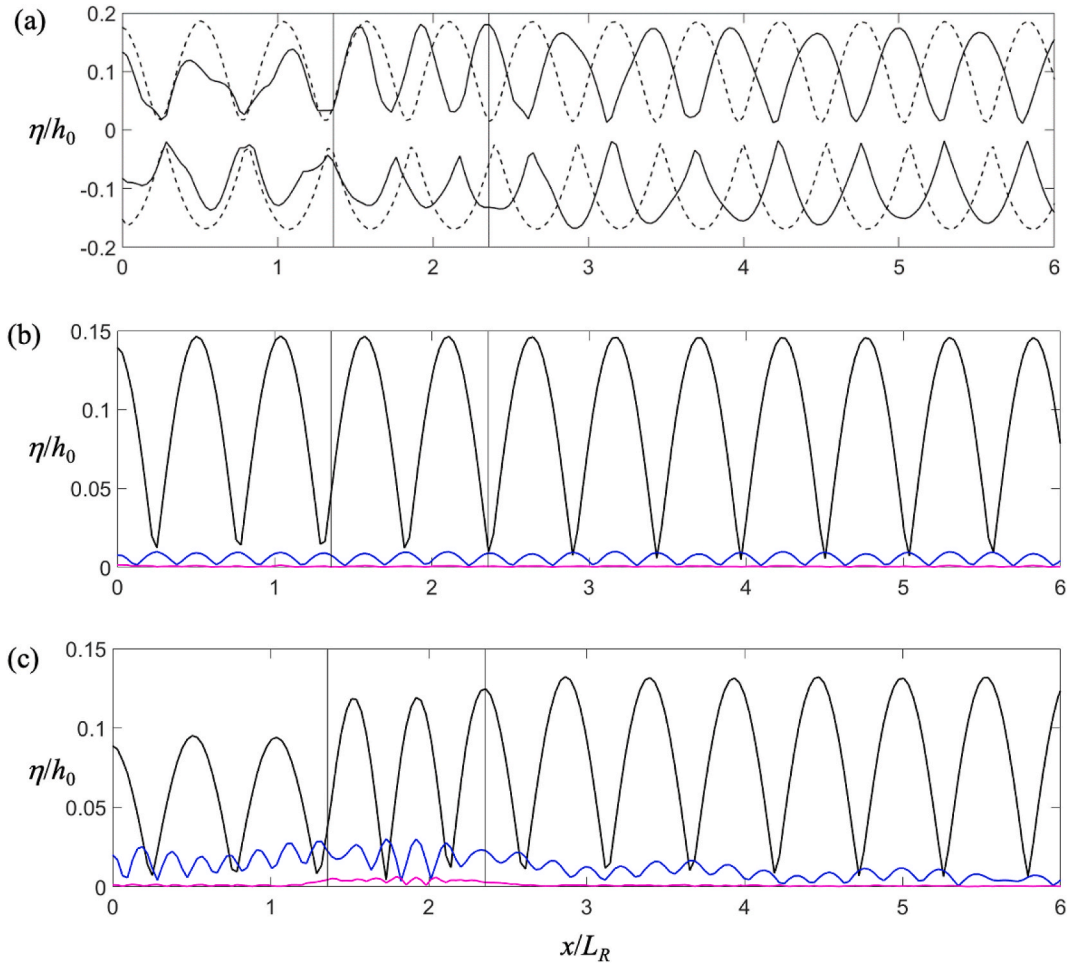

Fig. 6. Standing wave formation for the incident cnoidal wave with $m = 0.457$ at steady state: the wavelength λ is the same as the breadth of the submerged reef L_R ($\lambda = L_R$), and the location of the reef is indicated by the thin vertical lines. (a) wave envelopes for Case R1LA (with presence of reef), solid lines and Case LA (without presence of reef), dashed lines; (b) amplitudes of the fundamental harmonic component (black line), 2nd harmonic (blue line), 3rd harmonic (magenta line) with no presence of the reef (LA); (c) the same as (b) with presence of the reef (R1LA). (For interpretation of the references to colour in this figure legend, the reader is referred to the Web version of this article.)

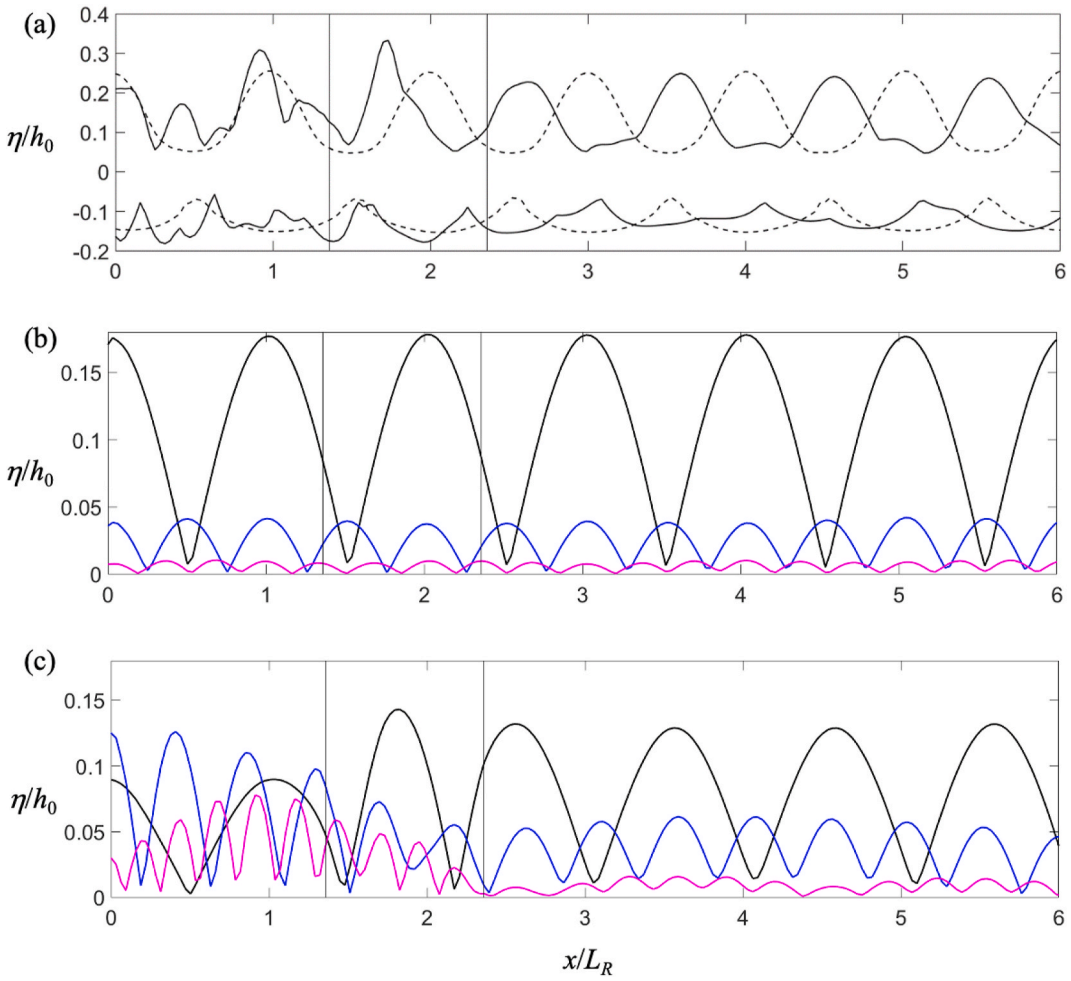

Fig. 7. Standing wave formation for the incident cnoidal wave with $m = 0.902$ at steady state: the wavelength λ is twice the breadth of the submerged reef L_R ($\lambda = 2L_R$), and the location of the reef is indicated by the thin vertical lines. (a) wave envelopes for Case R1LC (with presence of reef), solid lines and Case LC (without presence of reef), dashed lines; (b) amplitudes of the fundamental harmonic component (black line), 2nd harmonic (blue ine), 3rd harmonic (magenta line) with no presence of the reef (LC); (c) the same as (b) with the presence of the reef (R1LC). (For interpretation of the references to colour in this figure legend, the reader is referred to the Web version of this article.)

more complex than the ones seen for Case R1LA (Fig. 6a); the complex behavior is consistent with the laboratory observation for Case B (see Fig. 5b). The wave envelope is amplified across the lagoon, with the smaller peaks observed at locations corresponding to partial nodes in Case LC. This wave amplification extends to the reef span; the maximum elevation η_{max}/h_0 there is approximately 30% greater than the case of LC. The troughs, however, are not significantly different in magnitude to the ones seen for Case LC. This is in contrast to the comparisons made between Cases LA and R1LA (Fig. 6a), where a reduction of the envelope trough was observed. As with Cases LA and R1LA, the phase shift in wave envelope is caused by the presence of the reef, owing to the adjustment in phase speed there. The wave envelope formation in the lagoon and reef is in contrast to the uniform envelope shape seen in the offshore region. This uniformity in envelope is similar to the one seen for Case LC, albeit slightly distorted. The similar shape and amplitude imply the occurrence of 'almost' total wave reflection.

As shown in Fig. 7b, the fundamental harmonic amplitude of the standing cnoidal wave remains dominant across the domain. Contrary to Case LA (Fig. 6b), however, the higher harmonics for Case LC are more apparent due to the greater nonlinearity influence in the incident cnoidal waves with $m = 0.902$. When the reef is present, Fig. 7c exhibits that the offshore region presents uniform peaks for the fundamental harmonic, albeit with reduced magnitude from Case LC. This reduction is at the expense of a sustained increase in the 2nd harmonic. The 2nd harmonic amplitude further increases midway across the reef, and continuously grows up to a maximum at the end-wall of the lagoon, where it surpasses the fundamental harmonic amplitude. The influence of the higher harmonics in the lagoon is further supported by the enhanced amplitude for the 3rd harmonic across the lagoon, while remaining small in the offshore region. The active higher harmonics in the lagoon explain the complex wave activity in the lagoon observed during both the laboratory and numerical experiments. Interestingly, among the three cases examined here (R1LA, R1LC and R1LF), this case presents the highest amplification in higher harmonic response in the lagoon. Note that this is consistent with the finding in (Ohyama and Nadaoka, 1994) who reported that the higher harmonic amplitudes for transmitted waves over a submerged shelf is the highest when the width of the shelf is one half of the beat length over the shelf.

The envelopes for Cases LF and R1LF are shown in Fig. 8a; this is the case for the incident cnoidal wave with $m = 0.990$ and the wavelength is thrice the reef breadth ($\lambda = 3\ L_R$). As shown in Fig. 8a, the runup at the end-wall is practically not different between the cases without the reef (LF) and with the reef (R1LF), while the rundown is much more pronounced in R1LF: about 40% larger. The wave envelope in the lagoon is amplified due to the presence of the reef. As incident waves across a reef become longer, wave transmission is enhanced, resulting in higher wave actions on the lee side of the reef. The amplification in the lagoon extends to the reef span, with an anti-node observed at the inshore edge of

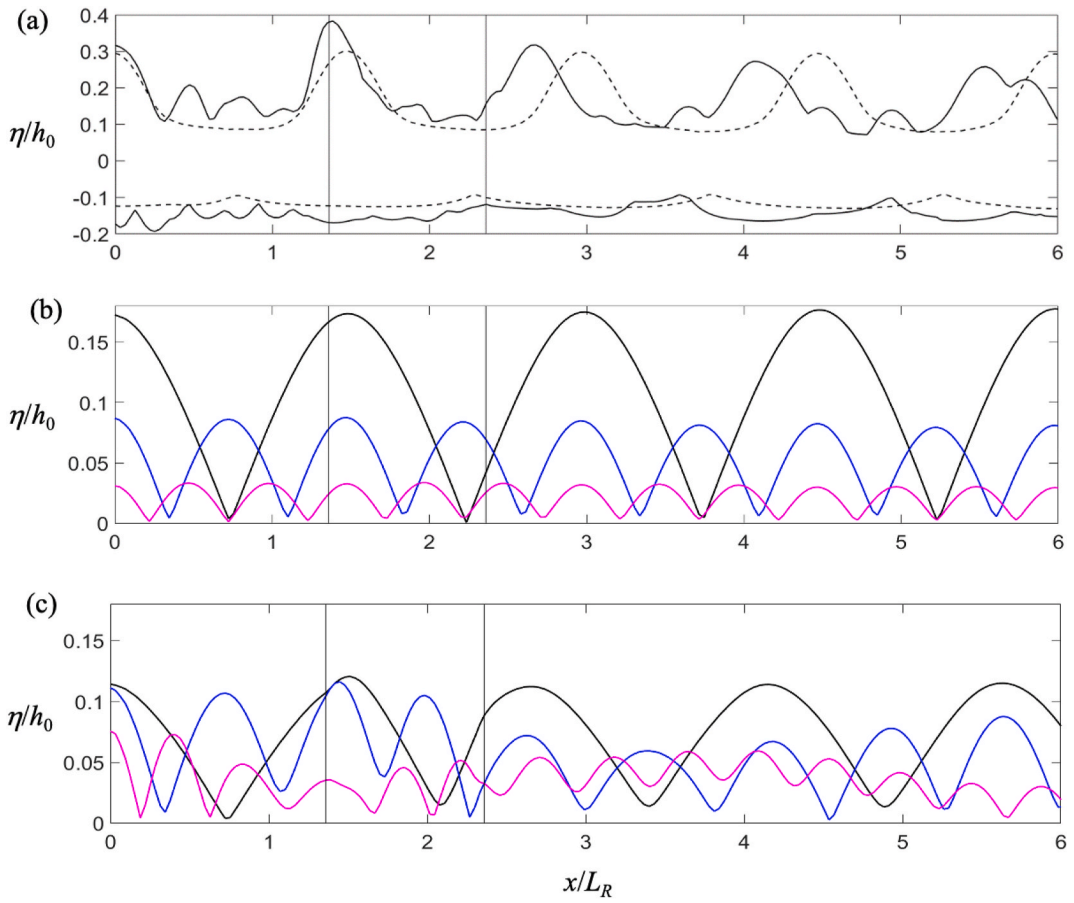

Fig. 8. Standing wave formation for the incident cnoidal wave with $m = 0.990$ at steady state: the wavelength λ is three times the breadth of the submerged reef L_R ($\lambda = 3L_R$), and the location of the reef is indicated by the thin vertical lines. (a) wave envelopes for Case R1LF (with presence of reef), solid lines and Case LF (without presence of reef), dashed lines; (b) amplitudes of the fundamental harmonic component (black line), 2nd harmonic (blue line), 3rd harmonic (magenta line) with no presence of the reef (LF); (c) the same as (b) with the presence of the reef (R1LF). (For interpretation of the references to colour in this figure legend, the reader is referred to the Web version of this article.)

the reef. As with Cases R1LA and R1LC, this lee edge of the reef demarcates the phase shift, which extends into the offshore extent. The phase shift is similar to the ones observed in Cases R1LC. The peak of the wave envelope formation in the offshore region resembles the envelope without the presence of the reef (about 7% difference between R1LF and LF).

The amplitude of the fundamental harmonic of the standing waves with no presence of the reef (Case LF) is shown in Fig. 8b. Compared with Case LA (Fig. 6b) and Case LC (Fig. 7b), the higher harmonics, in particular the 2nd harmonic, become more significant, as the parameter m of cnoidal waves becomes larger. The presence of reef does not significantly affect the uniformity in the fundamental harmonic component as shown in Fig. 8c. The higher harmonics in the lagoon is substantial; the amplitude of the 2nd harmonic is amplified and becomes comparable with that of the fundamental component. It is noted that, while the fundamental harmonic envelope is uniform in the offshore region, the 2nd and 3rd harmonics are varied gradually. This reflects the slowly changing offshore wave envelope shown in Fig. 8a. The reason for this behavior is not clear, but we conjecture that this might be resulted from the slowly varying energy exchange among harmonics that is triggered by the presence of the reef to the highly nonlinear ($m = 0.990$) and very long wave ($\lambda = 3\ L_R$).

The sustained magnitudes of the fundamental harmonic amplitude across the reef and into the lagoon region is attributed to the long incident waves passing over the low elevation reef. The failure of the reef to blunt the incoming wave energy is further supported by the reflection coefficient, K_r, in the offshore region, which is substantially lower than Cases R1LA and R1LC, as presented in Table 3. Note that the reflection coefficient of the fundamental harmonic component K_r is estimated at the offshore stretch that extends from the offshore edge of the reef to $x/L_R = 6.27$:

$$K_r = \frac{\eta_{max} - \eta_{\min}}{\eta_{max} + \eta_{\min}}, \tag{8}$$

where η_{max} is a maximum amplitude of the envelope (at the quasi-antinodes) and η_{min} is a minimum amplitude of the envelope (at the quasi-nodes). Note that the reflection coefficient K_r is calculated by treating the harmonic components being linear, though the present standing waves created by the incident cnoidal waves do not behave like linear waves, strictly speaking. Therefore, the values listed in Table 3 should be considered as a qualitative indicator. As it can be seen from Table 3, R1LF displays the lowest reflection coefficient value ($K_r = 0.792$) in comparison with $K_r = 0.908$ for R1LA and 0.892 for R1LC. This

Table 3
Reflection coefficients for illustrated cases.

Wave Case		K_r for fundamental harmonic amplitude
$\lambda/L_R = 1$, $m = 0.457$	LA	**0.937**
	R1LA	**0.908**
$\lambda/L_R = 2$, $m = 0.902$	**LC**	**0.943**
	R1LC	**0.892**
$\lambda/L_R = 3$, $m = 0.990$	**LF**	**0.968**
	R1LF	**0.792**

suggests that the energy in the incident fundamental component must be transferred to the higher harmonic components to form the reflected waves, and this trend is greater for the incident waves with larger values of m. It is noted that the similar procedure was attempted to obtain the reflection coefficients for the higher harmonic components. Unfortunately, such an attempt failed because the envelope of the higher-harmonic waves exhibits slow modulation; hence we could not determine the values of η_{max} and η_{min}. Because no such modulation in the higher harmonic components is detected for the cases without the presence of the reef (see Figs. 6b, 7b and 8b), we speculate that the modulation must be caused by the generation of noise in wavenumber created by the reef.

The wave amplification over the reef that is seen for the longer waves (Figs. 7c and 8c) was also reported by Christou et al. (2008), who examined the effects of progressive wave propagations over a submerged breakwater. They noted that as the wave evolves over the breakwaters, significant steepening and nonlinear amplification occurs. Christou et al. (2008) described the downstream wave activity as highly nonlinear, due to the combination of the generation of wave harmonics as well as the interaction between the free and bound wave components. These responses align with the present investigation in the standing wave formations, whereby complex and energetic wave activity is observed in the lagoon extent of the longer wave cases (Figs. 7a and 8a).

4.2. Maximum wave heights along cross-shore domain

The influence of the reef on the incident waves are examined in terms of the ratio of the maximum wave height $H_{\max}$ to the maximum wave height in the absence of the reef H^*. We examine the three notable locations: a) end-wall, b) lagoon and reef stretch, c) offshore extent. The ratio H_{max}/H^* is presented for several reef heights (shown in terms of reef height, D, normalized by the initial water depth, h_o) and the results are shown in Fig. 9.

At the end-wall (Fig. 9a), a clear correlation is seen between maximum wave heights $H_{\max}/H^*$ and reef height D/h_0, whereby the highest reef ($D/h_0 = 0.7$) results in the lowered maximum wave heights for all 5 wavelengths. The water column depth over the reef has a direct correlation to the wave heights at the end-wall. For each of the reef heights, as the waves become longer, the maximum wave heights at the end-wall increase as they overcome the submerged reef more efficiently. The exception is for the case $\lambda/L_R = 2$, where slight reduction from the above trend is noted. The maximum wave height $H_{\max}/H^*$ at the end-wall for the low reef heights ($D/h_0 = 0.508$ and 0.6) and long wavelengths ($\lambda/L_R = 2.5$ and 3) exceeds unity. This entails that the presence of reef not only fails to act as a buffer to the incident waves, but also has an adverse effect, resulting in an amplification at the end-wall. Fig. 9a shows that the presence of a reef with the height lower than 50–60% of the ambient water depth potentially becomes a threat towards longwave activity at the shore. Ramping up the reef height to 70% of the water column ($D/h_0 = 0.7$) only slightly attenuates the wave response at the wall for the longest incident wave case, $\lambda/L_R = 3$.

Along the lagoon and reef stretch (Fig. 9b), the maximum wave height remains unchanged ($H_{\max}/H^* \approx 1$) for all three reef heights for the case $\lambda/L_R = 1$. As the waves become longer for the reef height $D/h_0 = 0.508$ and 0.6, however, the amplification of the wave height results, i.e., $H_{\max}/H^* > 1$. For $D/h_0 = 0.7$, the wave height attenuates $H_{\max}/H^* < 1$ for the waves $\lambda/L_R = 1.5$ and 2, while the waves with longer wavelengths, $\lambda/L_R = 2.5$ and 3, retain amplified magnitudes above the baseline. Note that Abdul Khader and Rai (1980) suggested that, for the shorter waves over submerged breakwaters, a range of relative submergence of 43–66% of the water column is sufficient in reducing wave energy. This discrepancy with our findings must be attributed to the difference between their progressive waves and our standing wave formation behind the barrier.

In the presence of the lowest reef height, $D/h_0 = 0.508$, the offshore maximum wave height (Fig. 9c) is relatively uniform, close to unity, for all five wavelengths. Consequently, this indicates that the reef influence is localized to the immediate lagoon area. The effect of raising the reef height to $D/h_0 = 0.6$ is relatively insignificant in the offshore wave heights, while $D/h_0 = 0.7$ is effective in attenuating the offshore waves. Interestingly, the maximum wave heights for the cases of $\lambda/L_R = 2$ and 3 remain unchanged for all three reef heights. Consequently, for the case of very long waves, $\lambda/L_R = 3$, wave amplification is sustained across a majority of the cross-shore domain, from the shore, into the lagoon and

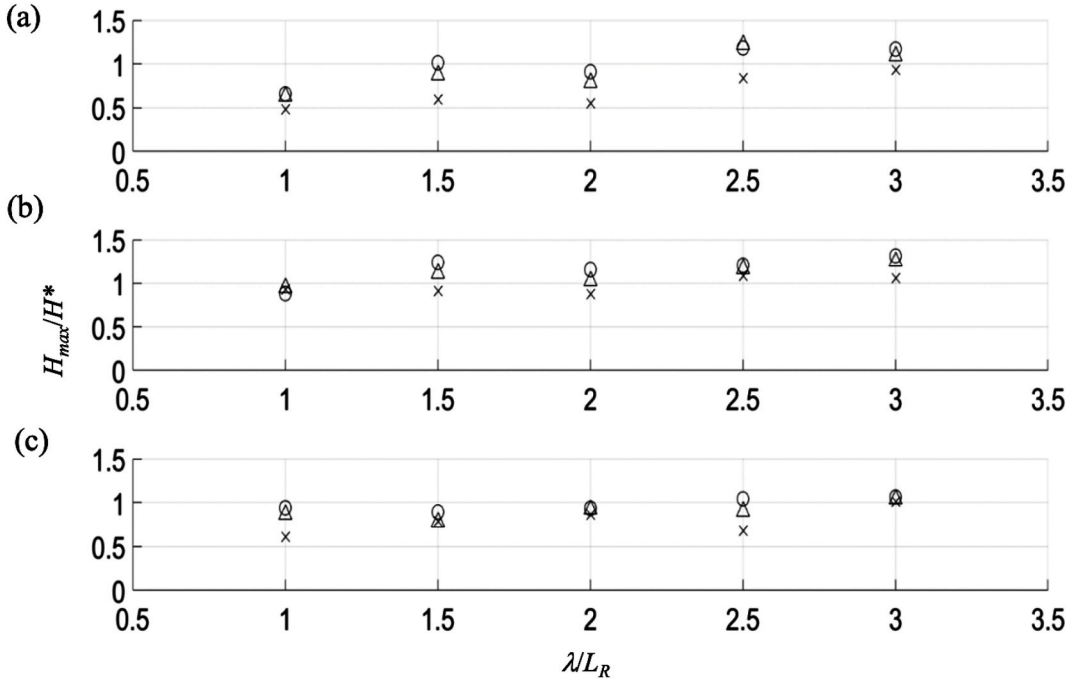

Fig. 9. Ratio of the maximum wave height influenced by the reef, H_{max}, to the maximum wave height in the absence of a reef, H^* at a) end-wall (x = 0), b) lagoon and reef stretch ($0 < x/L_R < 2.35$), c) offshore region ($2.35 < x/L_R < 79$) under the condition of the reef height D: ○, $D/h_0 = 0.508$; Δ, $D/h_0 = 0.6$; × , $D/h_o = 0.7$.

reef, and along the offshore region. Even with the higher reef, $D/h_0 = 0.7$, the presence of the reef is unable to effectively reduce the wave energy.

4.3. Phase shift

The wave phase is controlled at the end-wall because the antinode must be formed there. The normalized phase shift, φ, is taken as the difference in the anti-node locations between the cases with and without the presence of reef, and divided by L_R. The variation of the phase shift across the domain is shown in Fig. 10. As noted for the envelopes presented in Figs. 6a, 7a and 8a, a significant phase shift takes place primarily at the inshore edge of the reef, as shown in Fig. 10. The phase shift φ rapidly increases along the reef span, then slowly stabilizes outside the outer edge of the reef and remains nearly constant further offshore. Fig. 11 presents the mean values of the offshore φ, showing that a direct correlation exists between the magnitude of φ and the reef height. Increasing the height of the reef results in increased φ response in the wave envelope in the offshore region. For the reef heights of $D/h_0 = 0.508$ and 0.6, the maximum φ is observed for the case when the wavelength is twice the reef width $\lambda/L_R = 2$. The phase shift φ decreases as the waves become longer. Increase in φ is also observed for the largest reef height ($D/h_0 = 0.7$), with a maximum observed at $\lambda/L_R = 2.5$, followed by the reduced shift for $\lambda/L_R = 3$.

4.4. Effect of the lagoon breadth

Along with the effect of reef height, the effect of the lagoon breadth is examined, while the breadth of the reef remains the same. The ratio of the lagoon breadth L_L to the reef breadth L_R presented in Sec. 4.1, 4.2 and 4.3 is $L_L/L_R = 1.35$. Here we include the cases with additional reef-lagoon configurations: $L_L/L_R = 1$ and $L_L/L_R = 0.75$. The reef submergence of $D/h_0 = 0.508$ is used. The results are presented in Figs. 12–14 for the standing wave envelopes for waves $\lambda/L_R = 1$, 2 and 3, respectively.

For the shortest wave $\lambda/L_R = 1$, Fig. 12 shows that the lagoon breadth has an impact on the offshore portion of the wave envelope, albeit the smallest lagoon-breadth case (Fig. 12d) exhibits the envelope shape that is the most unaffected by the presence of the reef. The deformation in the envelope appears to be significant immediately offshore of the reef for the case of equal breadth in reef and lagoon (Fig. 12c). Amplification across the reef is also slightly elevated for this case. The wave attenuation inside the lagoon is seen for cases of $L_L/L_R = 1.35$ and 0.75 (Fig. 12b and d); on the other hand, no attenuation is observed for the case of equal lagoon and reef breadth $L_L/L_R = 1$ (Fig. 12c). For this resonant circumstance, the large amplification that is triggered at the reef, is sustained into the lagoon, and at the wall.

The uniform standing-wave envelopes are reproduced offshore for the case of $\lambda/L_R = 2$ as shown in Fig. 13. As seen in Fig. 13b, the case of the largest lagoon breadth, $L_L/L_R = 1.35$, portrays the most significant complex wave activity in the lagoon. The wave envelope attenuation in the lagoon is most pronounced for the smallest lagoon breadth (Fig. 13d), while the amplification along the reef/lagoon stretch is maximum for the case of equal lagoon and reef breadth (Fig. 13c): the same trend is found for the case of $\lambda/L_R = 1$ in Fig. 12c. Attenuation at the wall is most effective for the smallest lagoon breadth case (Fig. 13d).

Interestingly for the case of $\lambda/L_R = 3$, there are no obvious differences in wave envelope shape for all three reef-lagoon configurations as shown in Fig. 14. The waves that traverse the entire domain behave very closely to those that are deployed in an unobstructed domain (Fig. 14a).

The maximum wave amplification H_{max}/H^* is shown in Fig. 15. Note that H^* is the maximum wave height for the case without the presence of the reef. Fig. 15a shows the amplification at the end-wall, and indicates that the case of $L_L = L_R$ with $\lambda/L_R = 2$ yields the highest enhancement in wave height ($H_{max}/H^* = 1.275$), clearly surpassing the other cases. It is seen that for the configuration of $L_L = L_R$, the incident cnoidal wave with $\lambda/L_R = 2$ appears to reach a state of resonance. The large response at the wall for $L_L = L_R$ is also observed for the shortest wave ($\lambda/L_R = 1$), producing a slightly smaller maximum wave height response. On the other hand, the case of the long incident wave with $\lambda/L_R = 3$ results in similar maximum wave heights for all three reef-lagoon configurations. Fig. 15a shows that the most effective attenuation of the maximum wave height at the end-wall is for the reef-lagoon configuration $L_L = 1.35L_R$ for the shortest wave $\lambda/L_R = 1$. As was observed in Sec 4.2, adverse wave response is produced at the wall for long waves, which results from amplification above baseline magnitudes due to the presence of the reef. This maximum wave response is seen to further increase when the breadths of the reef and adjacent lagoon are comparable.

As shown in Fig. 15b, the wide majority of the cases along the lagoon/reef stretch present magnitudes greater than 1, implying amplification. A slight wave attenuation can be seen for the wavelengths, $\lambda/L_R = 1$ and 1.5, at specific reef-lagoon configurations ($L_L/L_R = 1.35$ and 0.75 for $\lambda/L_R = 1$ and $L_L/L_R = 1$ for $\lambda/L_R = 1.5$). For the longest wave $\lambda/L_R = 3$, there are no significant changes in the maximum

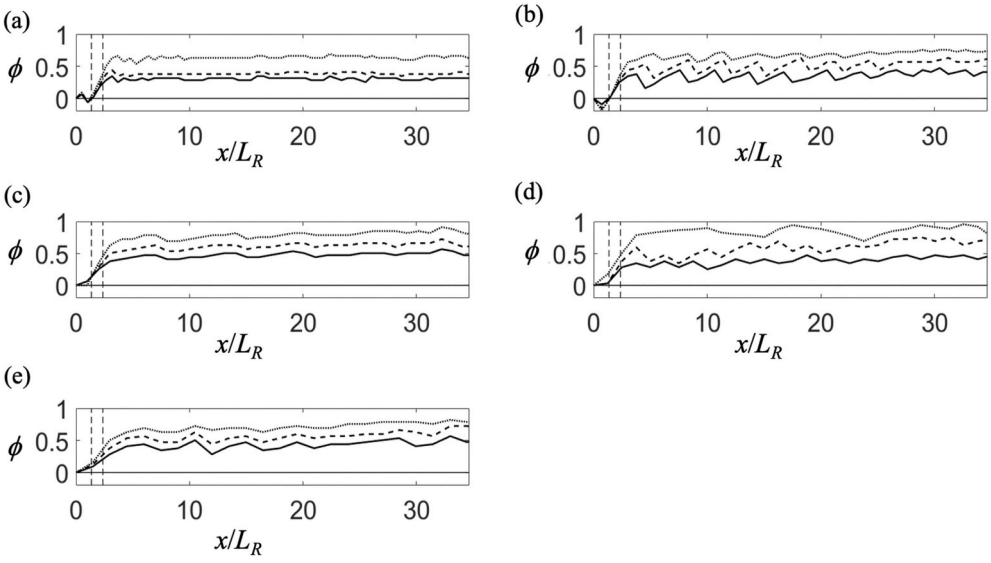

Fig. 10. Normalized phase shifts, φ, across different reef heights: $D/h_0 = 0.508$, solid bold line; $D/h_0 = 0.6$, dashed line; $D/h_0 = 0.7$, dotted line. The location of the reef is indicated by a pair of thin-dashed vertical lines. (a) $\lambda/L_R = 1$; (b) $\lambda/L_R = 1.5$; (c) $\lambda/L_R = 2$; (d) $\lambda/L_R = 2.5$; (e) $\lambda/L_R = 3$.

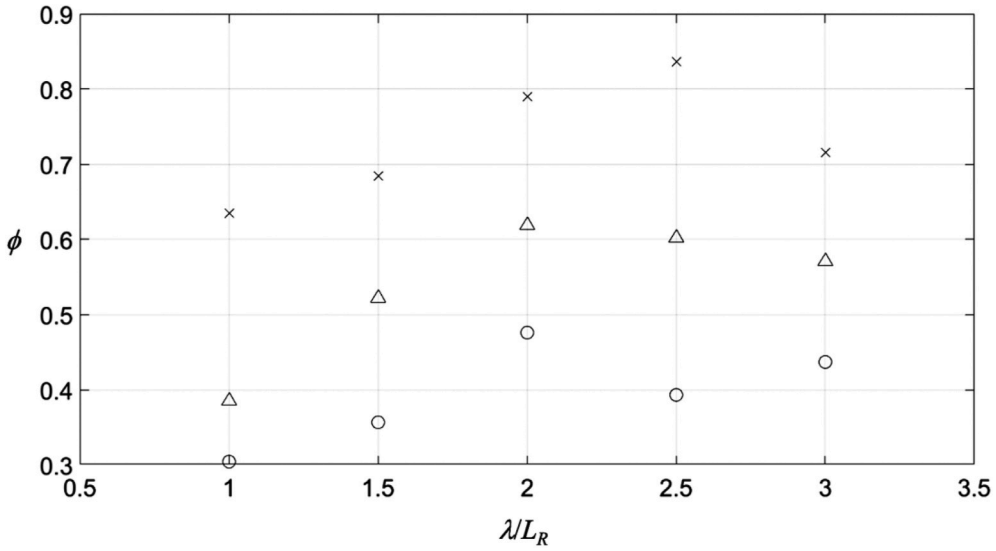

Fig. 11. Averaged phase shift φ in the offshore region ($2.35 < x/L_R < 79$) for different wavelengths, λ, with different reef heights D: ○, $D/h_0 = 0.508$; Δ, $D/h_0 = 0.6$; × , $D/h_0 = 0.7$.

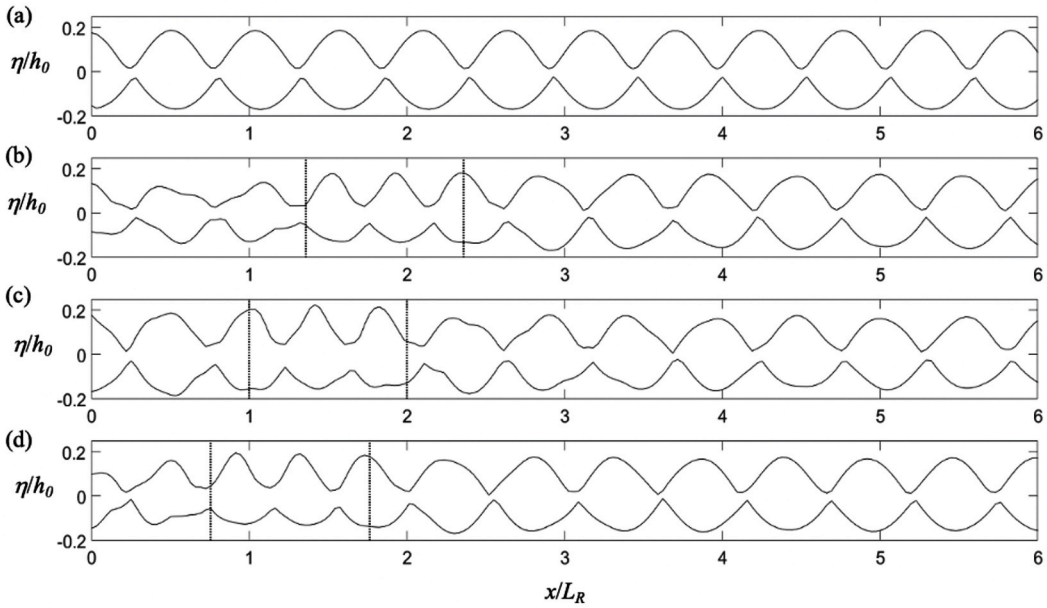

Fig. 12. Partially standing wave envelope for $\lambda/L_R = 1$ across different lagoon breadths. (a) no reef; (b) $L_L = 1.35L_R$; (c) $L_R = L_L$; (d) $L_L = 0.75L_R$. The location of the reef is indicated by vertical dotted lines.

wave height for the different lagoon breadths, resembling the response observed at the wall.

Fig. 15c shows that the maximum wave height in the offshore region exhibit near-identical magnitudes, close to unity. Hence, the reef to lagoon breadth ratio only significantly affects the wave envelope within the reef-lagoon region, while failing to influence the offshore stretch. A similar characteristic was found for the influence of reef submergence on the offshore wave envelope.

5. Conclusions

The present study aims at the exploration of long-wave response to the reef-lagoon bathymetry formed in front of the reflective wall. We consider the cases for the horizontal length scales of the reef and lagoon being comparable, motivated by the coral-reef features found in some of the tropical islands (see. Fig. 1). We focus on the incident waves which scale is comparable to the bathymetric scale. This bathymetric setup is different from previous studies related to the submerged breakwaters, where the breakwater breadth is shorter than the wavelength. The setup also differs from the problems of short wind waves intruding onto coral reefs. Because the reflective vertical end-wall is placed at the boundary, standing waves are formed. Based on the combination of our laboratory and numerical experiments, the following characteristics and behaviors of the longwave response under the standing-wave states are found.

- Owing to the presence of the reef, it is anticipated that the wave runup at the end-wall be reduced from that of the equivalent condition with no presence of the reef. It is indeed the case when the wavelength is comparable to the reef breadth. Nonetheless, the present results show that, for longer incident waves, the wave height

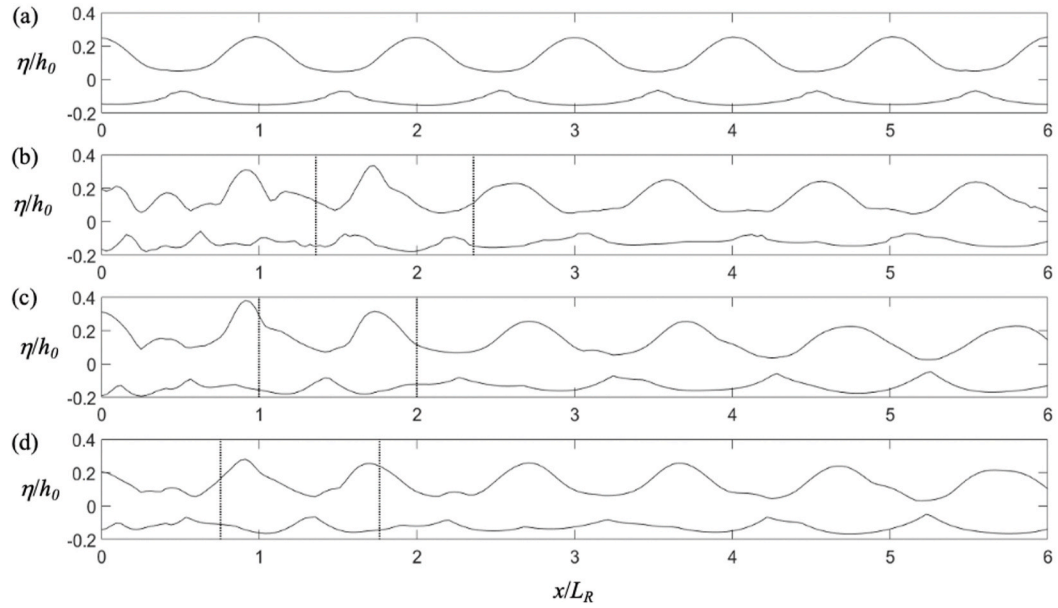

Fig. 13. Partially standing wave envelope for $\lambda/L_R = 2$ across different lagoon breadths. (a) no reef; (b) $L_L = 1.35L_R$; (c) $L_R = L_L$; (d) $L_L = 0.75L_R$. The location of the reef is indicated by vertical, dotted lines.

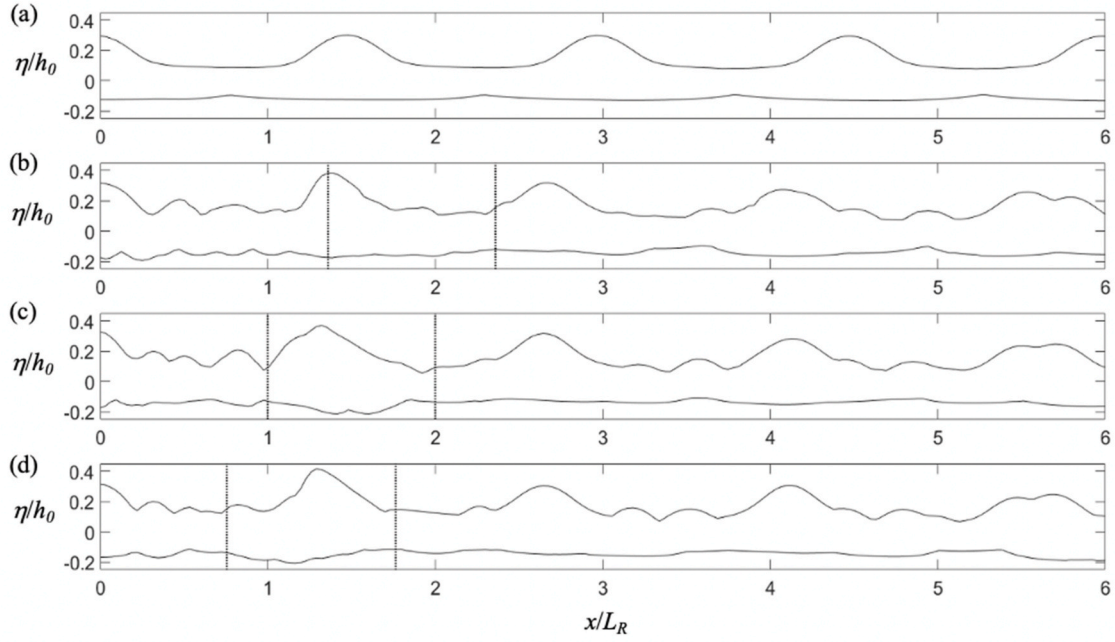

Fig. 14. Partially standing wave envelope for $\lambda/L_R = 3$ across different lagoon breadths. (a) no reef; (b) $L_L = 1.35L_R$; (c) $L_R = L_L$; (d) $L_L = 0.75L_R$. The location of the reef is indicated by vertical, dotted lines.

at the end-wall becomes greater than the case with no presence of the reef. Such an adverse effect is observed in the experiments when $\lambda/L_R > 2.5$. The adverse effect is most pronounced when the breadth of the reef and the adjacent lagoon are similar ($L_R \approx L_L$). Among the cases we examined, the maximum amplification in wave height is $H_{max}/H^* = 1.22$ when $\lambda/L_R = 2.5$ and $D/h_0 = 0.6$. The definitive reason for the increase is not clear, but it can be the occurrence of resonance associated with the disturbance of standing waves caused in the reef-lagoon system.

- Similar to the wave runup at the end-wall, when the wavelength is comparable to the reef breadth, the wave heights at the anti-nodes along the reef and lagoon span are smaller than the corresponding case without the reef. When the waves are longer, however, the presence of the reef and lagoon enhances the wave amplification. The wave heights at the antinodes become higher than at the end-wall: the maximum amplification in wave height is $H_{max}/H^* = 1.312$ when $\lambda/L_R = 3.0$ and $D/h_0 = 0.508$. It appears that the excessive amplification is caused by the irregular standing-wave formations inside the lagoon, which is attributed to the disruption of phase-locked harmonics of the incident waves, resulting in free waves in the lagoon. This conjecture is supported by the observations in the reef-lagoon stretch: (a) wave envelopes of the higher harmonic

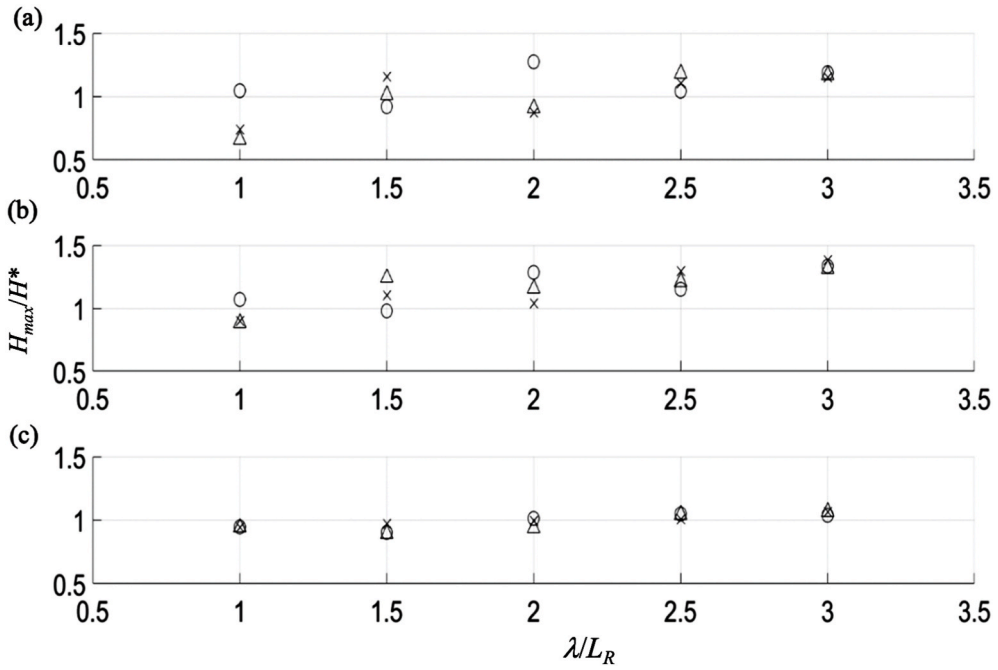

Fig. 15. Ratio of maximum wave height influenced by the reef, H_{max}, to the maximum wave height along domain in the absence of a reef, H^*: Δ, $L_L = 1.35L_R$; ○, $L_L = L_R$; × , $L_L = 0.75L_R$. a) end-wall (x = 0); b) lagoon and reef stretch (Δ, $0 < x/L_R \leq 2.35$; ○, $0 < x/L_R \leq 2.0$; × , $0 < x/L_R \leq 1.75$), c) offshore region (Δ, $2.35 < x/L_R \leq 79$; ○, $2.0 < x/L_R \leq 79$; × , $1.75 < x/L_R \leq 79$).

components are not orderly aligned with the fundamental harmonic component (Figs. 6c, 7c and 8c) and (b) the magnitude of the wave trough becomes greater than the case with no presence of the reef (Figs. 7a and 8a), showing that the wave form is no longer that of incident cnoidal wave. Our results highlight the possibility of broad reef-and-lagoon bathymetry configurations in worsening the wave climate from the baseline conditions (no reef) when the incident waves are longer than the length scale of the reef-lagoon bathymetry.

- The envelope formation of standing waves offshore does not change significantly from the corresponding base cases (no reef presence): the node and antinode amplitudes remain essentially the same, but their locations (phase) are shifted. Nonetheless, the results from the harmonic analysis reveal that the presence of the reef-lagoon system causes the enhancement of 2nd and 3rd harmonic components at the expense of fundamental component. This trend is greater for the longer incident waves: recall that, since we used cnoidal waves for the incident long waves, longer waves result in more nonlinear effects (i.e., large value of the elliptic parameter m).
- In all cases, the antinode formation occurs at the inshore edge of the reef. This location marks the origin of the phase shift from the envelope without the presence of a reef. A direct correlation is observed between the phase shift and reef height: the shallower the reef, the greater the shift. The phase shift is insignificant along the lagoon and reef span.

Our results highlight the occurrence of irregular standing wave formations in the stretch of broad lagoon-and-reef configurations and the possibility of worsening the wave height from the baseline conditions (no reef) when the incident waves are longer than the length scale of the reef-lagoon bathymetry. This complex and energetic wave field is limited in the region of the reef-lagoon system and the offshore wave condition is generally unaffected, except some phase shift and emergence of larger higher harmonic component.

CRediT authorship contribution statement

Vivek A. Bheeroo: conducted the experiments, Formal analysis, Writing – original draft, Writing – review & editing. **Harry Yeh:** proposed the research topic, Formal analysis, Writing – original draft, Writing – review & editing.

Declaration of competing interest

The authors declare that they have no known competing financial interests or personal relationships that could have appeared to influence the work reported in this paper.

Acknowledgements

The authors would like to acknowledge S. Harry for his help with laboratory experiments for the data presented herein, and an anonymous reviewer for careful reading and constructive suggestions.This work was supported by the US National Science Foundation (OCE-1830024).

References

Abdul Khader, M.I., Rai, S.P., 1980. A study of submerged breakwater. J. Hydraul. Res. 18, 113–121.
Adams, C.B., Sonu, C.J., 1987. Wave transmission across submerged near-surface breakwaters. In: International Conference on Coastal Engineering. American Society of Civil Engineers, pp. 1729–1738.
Baldock, T.E., O'Hare, T.J., Huntley, D.A., 2004. Long wave forcing on a barred beach. J. Fluid Mech. 503, 321–343.
Beji, S., Battjes, J.A., 1993. Experimental investigation of wave propagation over a bar. Coast. Eng. 19, 151–162.
Beji, S., Battjes, J.A., 1994. Numerical simulation of nonlinear wave propagation over a bar. Coast. Eng. 23, 1–16.
Christou, M., Swan, C., Gudmestad, O.T., 2008. The interaction of surface water waves with submerged breakwaters. Coast. Eng. 55, 945–958.
Dattatri, J., Raman, H., Shankar, N.J., 1979. Performance characteristics of submerged breakwaters. In: International Conference on Coastal Engineering. American Society of Civil Engineers, pp. 2153–2171.
Dick, T.M., Brebner, A., 1969. Solid and permeable submerged breakwaters. In: International Conference on Coastal Engineering. American Society of Civil Engineers, pp. 1141–1158.
d'Angremond, K., Van Der Meer, J.W., De Jong, R.J., 1997. Wave transmission at low-crested structures. In: International Conference on Coastal Engineering. American Society of Civil Engineers, pp. 2418–2427.

Eldeberky, Y., Battjes, J.A., 1995. Nonlinear coupling in waves propagating over a bar. In: International Conference on Coastal Engineering. American Society of Civil Engineers, pp. 157–167.
Ferrario, F., Beck, M.W., Storlazzi, C.D., Micheli, F., Shepard, C.C., Airoldi, L., 2014. The effectiveness of coral reefs for coastal hazard risk reduction and adaptation. Nat. Commun. 5, 1–9.
Goda, Y., Takeda, H., Moriya, Y., 1967. Laboratory investigation on wave transmission over breakwaters. Rep. Port Harbour Res. Inst. 13, 38.
Goring, D., Raichlen, F., 1980. The generation of long waves in the laboratory. In: International Conference on Coastal Engineering. American Society of Civil Engineers, pp. 763–783, 7.
Hardy, T.A., Young, I.R., 1996. Field study of wave attenuation on an offshore coral reef. J. Geophys. Res. 101, 14311–14326.
Huang, C.-J., Dong, C.-M., 1999. Wave deformation and vortex generation in water waves propagating over a submerged dike. Coast. Eng. 37, 123–148.
Johnson, J.W., Fuchs, R.A., Morison, J.R., 1951. The damping action of submerged breakwaters. Trans. Am. Geophys. Union 32, 704–p00704.
Kittitanasuan, W., Goda, Y., Shiobara, T., 1993. Deformation of nonlinear waves on a rectangular step. Coast. Eng. Japan 36, 133–153.
Ko, H.T.S., Yeh, H., 2018. On the splash-up of tsunami bore impact. Coast. Eng. 131, 1–11.
Lee, T.T., Black, K.P., 1978. The energy spectra of surf waves on a coral reef. In: International Conference on Coastal Engineering. American Society of Civil Engineers, pp. 588–608.
Li, F.C., Ting, C.L., 2012. Separation of free and bound harmonics in waves. Coast. Eng. 67, 29–40.
Longuet-Higgins, M.S., Stewart, R.W., 1960. Changes in the form of short gravity waves on long waves and tidal currents. J. Fluid Mech. 8, 565–583.
Longuet-Higgins, M.S., Stewart, R.W., 1964. Radiation stresses in water waves; a physical discussion, with applications. Deep. Res. Oceanogr. Abstr. 11, 529–562.
Losada, I.J., Silva, R., Losada, M.A., 1996. 3-D non-breaking regular wave interaction with submerged breakwaters. Coast. Eng. 28, 229–248.
Lowe, R.J., Falter, J.L., Bandet, M.D., Pawlak, G., Atkinson, M.J., Monismith, S.G., Koseff, J.R., 2005. Spectral wave dissipation over a barrier reef. J. Geophys. Res. 110, 1–16.
Massel, S.R., 1983. Harmonic generation by waves propagating over a submerged step. Coast. Eng. 7, 357–380.
Mei, C.C., 1983. The Applied Dynamics of Ocean Surface Waves. John Wiley & Sons, New Yrok, p. 740-740.
Monsalve, E., Maurel, A., Pagneux, V., Petitjeans, P., 2015. Propagation of nonlinear waves passing over submerged step. Phys. Procedia 70, 863–866.
Nwogu, O., Demirbilek, Z., 2010. Infragravity wave motions and runup over shallow fringing reefs. J. Waterw. Port, Coast. Ocean Eng. 136, 295–305.
Ohyama, T., Nadaoka, K., 1994. Transformation of a nonlinear wave train passing over a submerged shelf without breaking. Coast. Eng. 24, 1–22.
Péquignet, A.C.N., Becker, J.M., Merrifield, M.A., Aucan, J., 2009. Forcing of resonant modes on a fringing reef during tropical storm Man-Yi. Geophys. Res. Lett. 36, 20–23.
Péquignet, A.C., Becker, J.M., Merrifield, M.A., Boc, S.J., 2011. The dissipation of wind wave energy across a fringing reef at Ipan, Guam. Coral Reefs 30, 71–82.
Petti, M., Ruol, P., 1993. Laboratory tests on the interaction between nonlinear long waves and submerged breakwaters. In: International Conference on Coastal Engineering. American Society of Civil Engineers, pp. 792–803.
Rey, V., Belzons, M., Guazzelli, E., 1992. Propagation of surface gravity waves over a rectangular submerged bar. J. Fluid Mech. 235, 453–479, 6.
Seabrook, S.R., Hall, K.R., 1999. Wave transmission at submerged rubblemound breakwaters. In: International Conference on Coastal Engineering. American Society of Civil Engineers, 2000–2013.
Seelig, W.N., 1983. Laboratory study of reef-lagoon system hydraulics. J. Waterw. Port, Coast. Ocean Eng. 109, 380–391.
Tavakkol, S., Lynett, P., 2017. Celeris: a GPU-accelerated open source software with a Boussinesq-type wave solver for real-time interactive simulation and visualization. Comput. Phys. Commun. 217, 117–127.
van der Meer, J.W., Briganti, R., Zanuttigh, B., Wang, B., 2005. Wave transmission and reflection at low-crested structures: design formulae, oblique wave attack and spectral change. Coast. Eng. 52, 915–929.
Young, I.R., 1989. Wave transformation over coral reefs. J. Geophys. Res. 94, 9779.
Zheng, Y.H., Shen, Y.M., Tang, J., 2007. Radiation and diffraction of linear water waves by an infinitely long submerged rectangular structure parallel to a vertical wall. Ocean Eng. 34, 69–82.